ADVANCED OPTICAL MATERIALS
www.advopticalmat.de

In Situ and Ex Situ Luminescence Investigation of Rare Earth Layered Double Hydroxides Intercalated with Mellitate Anion

Ercules E. S. Teotonio, Giscard Doungmo, Jonas Ströh, Danilo Mustafa, Israel F. Costa, Hermi F. Brito, Aleksei Kotlov, and Huayna Terraschke**

This work reports the preparation by co-precipitation method of $[Zn_2Al_{0.95}:Ln_{0.05}(OH)_6](HMA)_{0.21}\cdot(H_2O)_x$, where x = 1.0–1.7 and Ln^{3+}: Sm^{3+}, Eu^{3+}, Gd^{3+}, Tb^{3+} and Dy^{3+}, doped trivalent lanthanide ions (Ln^{3+}) intercalated with mellitate (HMA^{5-}) anions in the interlayer gallery. The results indicate that the Ln^{3+} ions and the organic anion are effectively introduced into the material without significantly losing the structural properties of the layered double hydroxydes (LDH). In situ measurements reveal slight changes in the luminescent properties assigned to the nucleation and growth processes of the LDH. Ex situ experiments show that the photophysical properties also changed after the drying process, indicating significant interactions of the mellitate anion in the materials. LDH-HMA:Eu^{3+} and LDH-HMA:Tb^{3+} exhibit high luminescence intensity in the red and green spectral regions due to the $^5D_0 \rightarrow {}^7F_{0\text{-}6}$ and $^5D_4 \rightarrow {}^7F_{6\text{-}0}$ transitions, respectively. The LDH-HMA doped with different ratios Eu^{3+}/Tb^{3+} presenting emission colors from red to green are also investigated. Surprisingly, the unexpected afterglow blue luminescence from the LDH-HMA doped with Gd^{3+} ion is ascribed to the phosphorescence $T \rightarrow S_0$ transition. Finally, obtaining three red, green and blue luminophores based on the same type of material represents an effective strategy toward white-light emission realized by mixing three different LDHs materials based on Ln^{3+} ions.

1. Introduction

In the last decades, inorganic layered solids have drawn growing interest from both scientific and technological communities mainly due to their fascinating capability for adsorption and intercalation of chemical species as well as their swelling properties[1–3] Among this class of materials, LDHs have received particular attention in chemistry, materials science, and environmental sciences mainly due to their anion-exchangeability, structure memory effect, good biocompatibility, and low-cost of manufacture.[4,5] Therefore, LDHs have been of paramount importance as promising materials to solve the main challenges faced by modern society, including environmental issues and energy crises. For example, they have been extensively explored as functional materials in separation processes, drug carriers,[6] corrosion,[7] and protection,[8] as a platform to support aggregation-induced emission (AIE)-active acceptors,[9] good recyclability and promising material for oil–water separation,[10] photochemical cells for water oxidation process,[11] in batteries,[12] as long-term antimicrobial materials[13] and slow-release fertilizers.[14] Recently, LDHs-based smart luminescent materials have been investigated as anticounterfeiting materials, photosensitizers for photodynamic therapy (PDT), cell imaging, and sensors.[15]

From a chemical and structural point of view, LDHs consist exclusively of positive sheets formed by divalent and trivalent metal cations octahedrally coordinated by hydroxide ions whose charge is balanced by anions A^{n-} intercalated in their galleries. The mineral hydrotalcite, $Mg_6Al_2(OH)_{16}CO_3\cdot 4H_2O$, is

E. E. S. Teotonio, G. Doungmo, J. Ströh, H. Terraschke
Institute of Inorganic Chemistry
Christian-Albrechts-Universität zu Kiel
Max-Eyth-Str. 2, D-24118 Kiel, Germany
E-mail: teotonioees@quimica.ufpb.br; hterraschke@ac.uni-kiel.de

The ORCID identification number(s) for the author(s) of this article can be found under https://doi.org/10.1002/adom.202402187

DOI: 10.1002/adom.202402187

E. E. S. Teotonio
Department of Chemistry
Federal University of Paraíba
João Pessoa, PB 58051-970, Brazil

D. Mustafa
Institute of Physics, University of São Paulo
São Paulo, SP 05508-090, Brazil

I. F. Costa, H. F. Brito
Institute of Chemistry
University of São Paulo
São Paulo, SP 05508-900, Brazil

A. Kotlov
Photon Science at DESY
Notkestrasse 85, 22607 Hamburg, Germany

the natural representative of this class of materials in which the CO_3^{2-} anion in the interlayer space balances the positive charge. Due to the tunable composition of LDHs with hydrotalcite-like structure, their general chemical formula is usually represented as $[M^{2+}_{1-x}M^{3+}_{x}(OH)_2]^{x+}(A_{x/n}{}^{n-})\cdot mH_2O$, where m represents the number of interlayer water molecules. In this case, the most common modifications in the LDH involve different combinations of divalent (e.g., Mg^{2+}, Ni^{2+}, Mn^{2+}, Zn^{2+}, Cu^{2+}, Co^{2+}) and trivalent (e.g., Al^{3+}, Fe^{3+}, Cr^{3+}, and V^{3+}) metal cations. Trivalent lanthanide ions (Ln^{3+}) have also been used as co-doping metal ions. However, it should be highlighted that the M^{2+}/M^{3+} molar ratio should be between 1.5 and 4.0 to obtain a phase-pure LDH structure. In addition to carbonate, which has a high affinity for occupying the interlayer space, other inorganic anions, such as NO_3^-, SO_4^{2-}, OH^-, PO_4^{3-}, and Cl^- have been intercalated directly during the synthesis or later by ion-exchange method to obtain traditional LDHs. It is worth mentioning that the type and the number of these anions play an essential role in the interlayer spacing and, consequently, in the chemical and physical properties of this system.[16,17] LDHs have been usually prepared by co-precipitation, anion exchange, calcination-reconstruction, hydrothermal and microwave-assisted hydrothermal, electrodeposition, and steam coating methods.[18,19] However, more than one of these methods can be subsequently used to obtain a material with specific properties. In general, the chosen method is based on the form of the desired product and the type of anion that should be intercalated in their galleries. The co-precipitation method is one of the most used methods for preparing LDHs as powders because it involves a simple setup for one-pot syntheses and milder reaction conditions.

Based on their chemical and structural properties, LDHs have been widely used as an excellent platform for developing smart luminescent materials via the intercalation of organic molecules and coordination compounds or by introducing Ln^{3+} ions into the layered structure of the system. In particular, the insertion of organic molecules capable of forming hydrogen bonds with the structure of the layered material may minimize the fast non-radiative decay processes because these strong interactions reduce intramolecular motions. In this vein, benzene dicarboxylic acid derivatives have received special attention as guest molecules because the n-π^* transitions can increase spin-orbit coupling, as well as the interactions among carboxylate groups with the material can contribute to the shift of energies and increase the emission lifetimes of the excited states of these molecules.[20]

Despite remarkable achievements in LDHs-based organic fluorescent and phosphorescent molecules, some practical applications require luminophores that exhibit pure emission colors in the visible region. The most straightforward alternative to overcome this problem is preparing LDHs doped with Ln^{3+} ions in the metal hydroxide sheets. Upon excitation in the UV region, materials containing these metal ions exhibit characteristic narrow emission bands related to the intraconfigurational-4f transitions.[21] For example, pure emission colors in the red and green regions may be obtained due to the $^5D_0 \rightarrow {}^7F_J$ and $^5D_4 \rightarrow {}^7F_J$ transitions (J = 0, 1, 2, 3, 4, 5 and 6) of the Eu^{3+} and Tb^{3+} ions, respectively. However, multiphonon relaxation processes due to OH groups in the LDH can contribute to luminescence quenching, especially in the case of the Eu^{3+} ion. In addition, 4f-4f transitions in the lanthanide ions are forbidden by parity Laporte's rule, so the direct excitation using common excitation sources (e.g., UV lamp) is usually limited.[22] In this regard, many research studies have explored the insertion of neutral or anionic coordination compounds of Ln^{3+} ions containing luminescence-sensitizing ligands or by LDH-doped lanthanide ion with simultaneous insertion of an efficient antenna ligand in the interlayer gallery.

In this context, highly photoluminescent doped materials Zn_2Al-LDH:Eu^{3+} intercalated with different β-diketonate anionic ligands (acac and tta) and with 1,3,5-benzenetricarboxylate (BTC) were reported by Morais and co-workers.[23] It also compared the luminescent properties of LDH intercalated with trimesate (benzene-1,3,5-tricarboxylate, BTC), trimellitate (benzene-1,2,4-tricarboxylate, TLA), terephthalate (benzene-1,4-dicarboxylate, TERE), isophthalate (ISO) and nitrilotriacetate (NTA), which show interactions between the coordination of the carboxylate ligands and the Eu^{3+} ion. Therefore, a less centrosymmetric chemical environment produces higher radiative decay rates as compared with materials containing NO_3^- in the interlayer gallery.[24,25] Furthermore, the dependence of basal spacing on the structural properties of dicarboxylate anions in the interlayer has also been extensively investigated.[26,27] Recently, LDH nanotubes doped with Ln^{3+} ions containing BTC^{3-} anion have been designed and synthesized by the soft-templating strategy using non-ionic Pluronic P-123 worm-like micelles as structure-directing agents. The organic anion included in the 1-nanometre-wide micropores has acted as a luminescence sensitizer for Ln^{3+} ions. Due to their high surface area, LDHs nanotubes interact with CdTe quantum dots, generating new highly luminescent materials.[28,29]

Another promising molecule type for obtaining smart luminescent LDH materials is the highly charged aromatic carboxylate anions, presenting a charge equal to or higher than −4. However, the intercalation of these systems into LDH has been rarely investigated. On the other hand, the syntheses and spectroscopic properties of their isolated complexes have been significantly addressed in the literature.[30–35] Among these ligands, pyromellitate anions (PMA^{4-}) have been intercalated into MgAl-LDH yielding a material with exceptional performance in the adsorption of uranium cation U^{6+}.[36] This ligand has also been used to prepare different nanocomposites for heterogeneous catalysis[37,38] and as an efficient treatment of aromatic pollutants.[39] However, to the best of our knowledge, only one study involving the formation of LDH and Mellitic acid (MA) has been reported in the literature.[40] Furthermore, no studies focusing on the luminescent properties of this organic acid and its derivative anions in LDHs containing Ln^{3+} ions have been reported so far.

Mellitic acid (or 1,2,3,4,5,6-benzenehexacarboxylic acid) may be naturally found in the mellite mineral of formula $[Al(H_2O)_6]_2\cdot C_{12}O_{12}\cdot 4H_2O$. Due to their structural characteristic of an aromatic core with six carboxylate groups, MA has been applied as a platform for self-assembly of 3D networks, forming several solid solutions containing MA^{2-} and MA^{4-} anions with cations from aromatic or aliphatic amines. It was pointed out that the intermolecular hydrogen bonding and the charge of MA^{n-} anions play an essential role in the formation of extended ribbons or sheets.[41,42] In the coordination chemistry field,

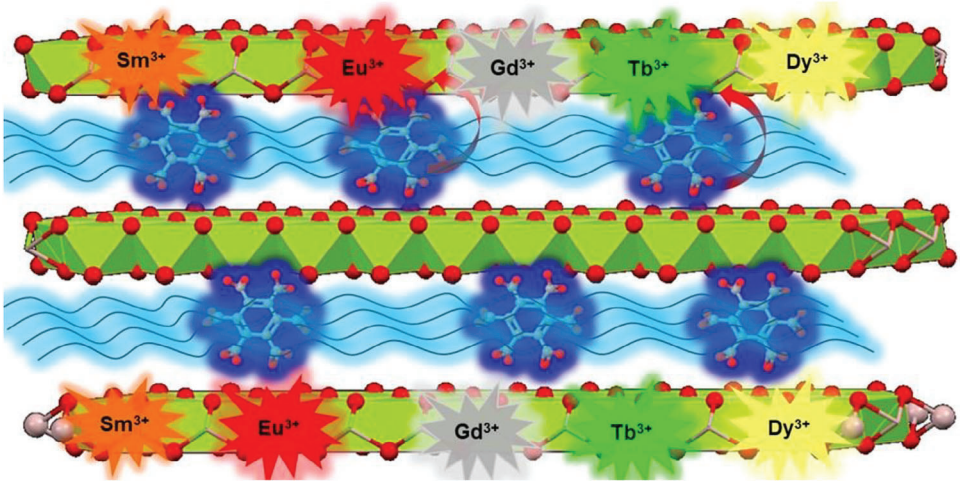

Figure 1. LDH-doped Ln^{3+} ions with mellitate anion (MA) in the interlayer gallery.

mellitates are very attractive owing to both the presence of several coordination sites and the possibility of different coordination modes characteristic of the carboxylate groups. Consequently, metal-organic frameworks (MOFs) with different morphologies are expected to form. Indeed, many transition metal, lanthanide, and actinide compounds contain mellitate as ligands.[30,35,43–45] However, the steric hindrance among carboxylate groups, the difficulty of synthesis, and the exceptional ability of mellitate to form intermolecular hydrogen bonding have been pointed out as some aspects that reduce the ability to coordinate strongly with the metal ions. In many compounds, mellitate is uncoordinated to the metal ions, or only a few of its carboxylate groups are coordinated, forming aqua complexes and highly hydrated coordination compounds. Therefore, its complexes are less investigated than those containing aromatic di- and tricarboxylic acids.

Here, LDHs doped with trivalent lanthanide ions (Ln^{3+}: Sm^{3+}, Eu^{3+}, Gd^{3+}, Tb^{3+}, and Dy^{3+}) have been successfully prepared by the co-precipitation method containing mellitate anion between the brucite-like layers (**Figure 1**). In situ and ex situ photophysical measurements reveal information about the formation mechanism of the materials expressing changes in the lanthanide chemical environment under the drying and thermal treatment. In addition to the highly red and green emission intensities exhibited by the Eu^{3+} and Tb^{3+}-doped materials, the spectral data shows an unusual blue emission for the LDH containing Gd^{3+} ion, even at room temperature. Another fascinating property this material presents is the emission afterglow, which can be observed even by the naked eye. Interestingly, changes in the interactions involving organic anion with interlayered water molecules and the hydroxide groups of the LDH structure are likely the key to the observed photophysical phenomenon. The lanthanide luminescence sensitization by the mellitate anion, as well as the possible energy transfer between different lanthanide ions, were targets of this study. The results were correlated with the electronic structures of the energy-donating and accepting species, as well as their positions in the material structure. Extrinsic quantum yields (Q_{Ln}^{L}) for LDHs doped with Eu^{3+} and Tb^{3+} ions were experimentally determined. Additionally, photophysical properties of the LDH doped with Eu^{3+} were quantitatively analyzed based on the experimental values of radiative (A_{rad}) and non-radiative (A_{nrad}) spontaneous emission coefficients, Judd–Ofelt intensity parameters Ω_λ ($\lambda = 2$ and 4) and intrinsic quantum yields (Q_{Ln}^{Ln}), allowing a deeper understanding of the luminescent properties of the LDH-Ln doped materials. This study demonstrated that a full-color material may be prepared by mixing LDH doped with Eu^{3+}, Gd^{3+}, and Tb^{3+} ions, and its luminescence color could be finely tuned by the ratio of the precursors. Therefore, this work contributes to the understanding and establishing new synthesis parameters in designing additional functional layered materials.

2. Methodology

2.1. Synthesis of LDHs Doped with Trivalent Lanthanide Ions

Layered double hydroxides with the general formula $[Zn_2Al_{1-x}:Ln_x(OH)_2]HMA$, where x = 0.05 or 0.15, and Ln: Sm^{3+}, Eu^{3+}, Gd^{3+}, Tb^{3+} and Dy^{3+}, were prepared by the co-precipitation, following the procedure described by Morais.[29] Considering that the reactions with different lanthanide ions were carried out using the same method, the preparation of the material doped with 5% of the Eu^{3+} ion (x = 0.05) is described as representative. Initially, 20 mL of an aqueous solution was prepared containing ≈3.9664 g of $Zn(NO_3)_2{\cdot}6H_2O$, 2.3734 g of $Al(NO_3)_3{\cdot}9H_2O$ and 0.1426 g of $Eu(NO_3)_3{\cdot}6H_2O$, which is equivalent to a molar ratio of 2:0.95:0.05. This solution was placed in an automatic titrator (Mettler Toledo GmbH, Gieβen, Germany). Then, 50 mL of a NaOH solution (≈1 mol L^{-1}) was also prepared and inserted into another position of the titrator. Subsequently, ≈0.1311 g of mellitic acid (MA) was dissolved in 65 mL of distilled water and placed in the reactor under magnetic stirring (Figure S1, Supporting Information). The pH of this solution was initially adjusted to 7.0. It should be noted that the solution in the reactor was continuously purged with nitrogen gas to avoid the formation of layered hydroxide containing the carbonate ion in the interlamellar region. Then, the pH and turbidimetry sensors were inserted into the reactor,

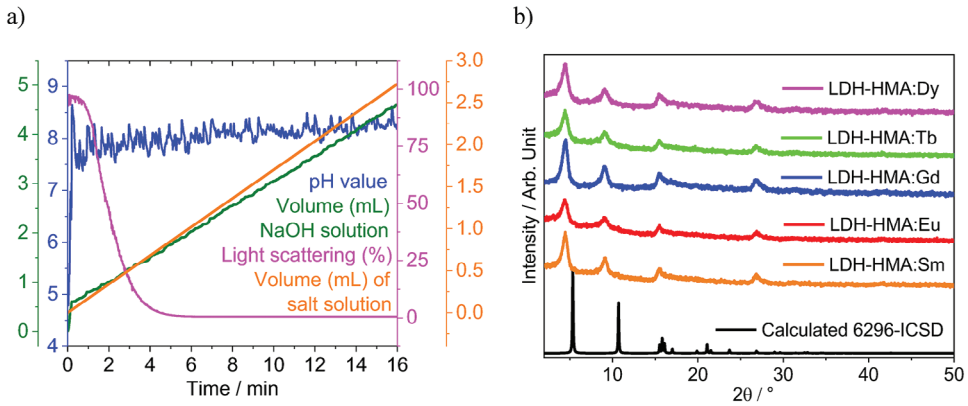

Figure 2. a) Time dependence of the pH (blue line), the dosed volume of the basic solution (green line), scattered light intensity at 365 nm (magenta line) and dosed volume of the salt solution (orange line), during the synthesis of sample LDH-HMA:Sm5% and b) X-ray diffraction patterns of the samples LDH:Ln5%-MA materials (Ln: Sm^{3+}, Eu^{3+}, Gd^{3+}, Tb^{3+} and Dy^{3+}).

while an optical fiber for excitation and emission acquisitions was placed on the outside of the reaction vessel. Finally, 3.33 mL of the salt solution was added to the reactor at a rate of 0.17 $mL{\cdot}min^{-1}$, maintaining the pH value at ≈8.0 by simultaneously adding the NaOH solution. During the whole reaction period, the temperature was maintained at ≈298 K. After this period, the resulting precipitate was centrifuged, washed several times with distilled water, and dried in an oven at 60 °C for ≈24 h.

2.2. Synthesis of Mixed Eu^{3+} and Tb^{3+} Doped LDHs

Layered double hydroxides doped with both Eu^{3+} and Tb^{3+} ions were prepared with the aim of investigating the intramolecular energy transfer processes in LDHs $[Zn_2Al_{0.95}:Eu_{0.05-y}:Tb_y(OH)_2]MA$. In this case, the total concentration of lanthanide ions was maintained at 5%, varying only the proportion between Eu^{3+} and Tb^{3+} ions (where y = 0.005; 0.01 and 0.025, which correspond to Tb:Eu molar ratios in percentages equal to 10, 20 and 50%, respectively.

3. Results and Discussion

The results of the in situ analyses shown in **Figure** 2a provide access to the first minutes of the reaction formation of LDH-HMA:Sm5%, during the addition of the solution of zinc, aluminum, and samarium salts to the reactor containing mellitic acid, simultaneously with the addition of NaOH solution for pH control. Already at 0.75 min a strong decrease in light transmission is observed, which indicates a strong increase in turbidity within this reaction time. As previously reported by Doungmo and co-workers,[46] this feature may be explained by increased concentration on the nucleation and growth processes. In this case, a critical supersaturation is suddenly achieved, and particle growth commences.

The X-ray diffraction patterns (PXRD) of the LDH-HMA:Ln5% materials (Ln: Sm^{3+}, Eu^{3+}, Gd^{3+}, Tb^{3+}, and Dy^{3+}) are shown in Figure 2b. It is interesting to note that the most intense Bragg peaks in the powder XRD diffractograms are those at 2θ values at ≈4.4, 9.1, and 15.4°, assigned to the planes (003), (006), and (009) of the hydrotalcite structure, respectively. Although heterogeneous materials containing lanthanide complexes of some dicarboxylate anions used to balance the negative charge of the LDH material have been reported in reference,[27] only Bragg peaks ascribed to the LDH may be observed in PXRD diffractograms. These data suggest that the intercalation of the homogenous materials containing intercalated MA^{n-} anion has been successfully obtained. Despite the high coordinating ability of the mellitate ligand to Ln^{3+} ions, strong intermolecular interactions between the various carboxylate groups of this organic anion with water molecules and hydroxide groups of the material likely play the most important role in stabilizing this anion in the interlayer gallery, preventing the formation of coordination polymers. Intercalation of the layers with MA^{n-} anion may be supported by lower angle shifts for the reflections due to the (003) and (006) planes, as compared to calculated data for hydrotalcite 6296-ICSD.[47] Based on the Bragg law and considering the positions of diffraction reflections, the basal distances (d) were also determined. Although the results show an increase in the basal distance from 7.6 to ≈9.0 Å, they are small compared to materials containing other carboxylates.[27,48] In this case, only a minor perturbation on the ZnAl-LDH structure is expected when the NO_3^- or CO_3^{2-} anions are replaced by MA^{n-} anion in the interlayer gallery. Two factors can contribute to this interesting result: 1) the higher charge of the MA^{n-} anion leads to a balance of the positive charge from hydroxide layers with a lower molar quantity of counterion and 2) when considering the planar structure of the organic ligand, some of these anions may also assume an almost parallel orientation to the hydroxide layers. It is worth mentioning that parallel orientation of MA^{n-} anion without significant loss of interactions of their carboxylate groups with metal ions and hydroxide groups on the surface of these layers may be adopted. Moreover, these MA^{n-} anion carboxylate groups can undergo torsions, acquiring an out-of-plane arrangement of the benzene ring.

The chemical compositions of the LDH-HMA:Ln^{3+} samples (Zn^{2+}, Al^{3+}, and Ln^{3+}) were determined based on CHN elemental analysis and the metal contents by using the ICP-OES technique (**Table** 1). The absence of nitrogen in these materials suggests a

Table 1. CHN Elemental, ICP-OES, and thermogravimetric data for the Zn_2Al-LDH:Ln^{3+} (wt%) materials.

Sample	%Zn^{2+}		%Al^{3+}		%Ln^{3+}		%C		%H		% residue at 900°C	
	Exp.	Calc.	Exp.	Calc.	Exp.	Calc.	Exp.	Calc.	Exp.	Calc.	Exp.	Calc.
LDH-HMA:Sm	37.06	35.92	6.36	7.04	2.45	2.06	8.39	8.14	2.71	2.52	58.91	62.26
LDH-HMA:Eu	36.00	35.74	6.31	7.01	2.00	2.08	8.42	8.36	2.73	2.52	59.23	60.49
LDH-HMA:Gd	35.87	35.49	6.30	6.96	1.67	2.13	8.66	8.57	2.72	2.50	61.20	61.21
LDH-HMA:Tb	33.60	35.39	6.06	6.94	2.41	2.15	8.22	8.66	2.75	2.49	58.90	60.68
LDH-HMA:Dy	34.95	35.67	6.04	6.99	2.24	2.22	8.19	8.37	2.97	2.51	57.77	62.57

higher affinity for inserting a highly charged MA^{n-} anion, which balances the positive charge of the LDH metal hydroxide sheets. The elemental analysis data suggest that there is no carbonate anion anchored to the materials, leading to ≈1/5 mellitate anion per unit $[Zn_2Al_{0.95}:Ln_{0.05}(OH)_6]^{n-}$. Although mellitate anion can acquire different values of negative charges, our results agree with the presence of the HMA^{5-} anion.

The thermogravimetric curves of the LDH-HMA:Eu doped materials recorded in the 25–900 °C temperature interval under a synthetic air atmosphere are presented as representative (**Figure 3a**). The TGA curves for the analogous materials with Sm^{3+}, Gd^{3+}, Tb^{3+}, and Dy^{3+} are shown in Figure S2, Supporting Information. As noted, these curves exhibit similar decomposition profiles, indicating that Ln^{3+} ion exchange does not significantly affect the materials' thermal stability or decomposition process. The first thermal decomposition from 25 to 168 °C, corresponding to a weight loss of ≈7% may be attributed to the dehydration process due to the release of surface adsorbed and interlayer water molecules. This finding indicates that ≈1.4 water molecules per unit $[Zn_2Al_{0.95}:Ln_{0.05}(OH)_6]^{n-}$ are slightly bonded in the LDH structure. A similar number of water molecules were found for LDHs intercalated by aliphatic dicarboxylate anion, as reported by Texeira and co-workers.[34] Based on these data and those from the CHN results, an idealized chemical formula $[Zn_2Al_{0.95}:Ln_{0.05}(OH)_6](MA)_{0.21}\cdot(H_2O)_x$ (where x is found between 1.0 and 1.7) may be proposed for the prepared LDH-HMA:Ln materials. After this temperature range, consecutive thermal decomposition events are also observed[40] at ≈500 °C, in which those between 168 and 350 °C are mainly assigned to the condensation of hydroxyl groups in the hydroxide sheets of the brucite-like octahedral layers. The dehydration and dehydroxylation processes were confirmed by DTA profiles as endothermic peaks (Figure 3a).[41] The final and most pronounced mass loss event may be attributed to intercalated HMA^{5-} anion decomposition. In the DTA curve, the final event is represented by an endothermic peak ≈445 °C. The remaining material (mixed metal oxides) corresponds to 60% of the starting sample.[42]

The infrared absorption spectra of the LDH-HMA:Ln doped materials recorded in the spectral range from 4000 to 400 cm^{-1} (Figure 3b) exhibit characteristic vibrational bands of the LDH structure, such as the bands ≈445 and 675 cm^{-1}, which may be ascribed to the deformation mode HO-Al-Zn-OH and the translation mode of Al–OH, respectively. The absence of the intense absorption band at 1700 cm^{-1} suggests that almost all carboxylic groups of the mellitate anion intercalated in the ZnAl-LDH material are deprotonated,[49] reinforcing the elemental analysis results for the existence of the HMA^{5-} anion. The bands at 1570 cm^{-1} may be attributed to the asymmetric stretching vibrations of COO^- groups, whereas those bands ≈1421 and 1331 cm^{-1} may be assigned to the symmetric stretching vibrations of the same groups. In addition, the broad absorption bands in the spectral region between 3300 and 3600 cm^{-1} are due to the O-H stretching modes from interlamellar water molecules and OH groups in the brucite-like layers. This behavior confirms the differences among the carboxylate groups from mellitate anions and their different coordination modes to the metallic centers in the hydroxide sheets. Furthermore, this anion can also form hydrogen bonding with water molecules or hydroxides in the structure of LDHs, leading to significant differences among the carboxylate vibrational modes.

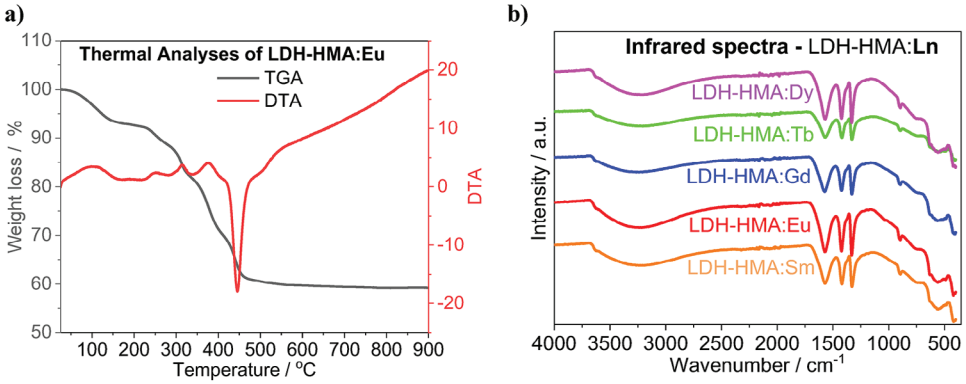

Figure 3. a) Thermogravimetric (TGA) and differential thermogravimetric (DTA) curves for the samples Zn_2Al-LDH:Eu (LDH-HMA:Eu) and b) Infrared spectra of the Zn_2Al-LDH:Ln (LDH-HMA:Ln) materials containing MA as anion (Ln: Sm, Eu, Gd, Tb and Dy).

The diffuse reflectance spectra (DRS) of the LDH-HMA:Ln^{3+} samples (after drying at 60 °C) recorded in the range from 250 to 500 nm (Figure S3, Supporting Information) are characterized by two overlapped broad absorption bands presenting a shoulder ≈295 nm (33 898 cm^{-1}) that may be attributed to the $S_0 \rightarrow S_1$ transition of the mellitate anion. The similarity between the spectral profiles for LDHs doped with different Ln^{3+} ions suggests that the mellitate anion has the same electronic structure in these materials. This result corroborates those obtained from infrared absorption spectra and thermogravimetric analyses, indicating that this organic anion exhibits similar interactions with the groups in LDH structure. Additionally, a comparison between DRS for LDH-HMA:Eu^{3+} and LDH-HMA:Gd^{3+} materials suggests that no ligand-to-metal energy transfer (LMCT) band is observed, which is usually found at lower energy spectral regions. In this case, the main pathway for the luminescence quenching process of lanthanide ions in these systems must involve the multiphonon relaxation mechanism.

3.1. Photophysical Properties

3.1.1. In Situ Luminescence Behavior

Unlike compounds with other lanthanide ions, the 4f-4f transitions are not observed in the visible region for the Gd^{3+} ion. Its first excited level $^6P_{7/2}$ lies at ≈32 000 cm^{-1} above ground level $^8S_{7/2}$. In this case, organic ligands with triplet states with too high energy are usually not found to promote an efficient luminescence sensitization for Gd^{3+} ions via the intramolecular ligand-metal energy transfer process. Therefore, the photophysical properties of Gd-compounds may provide information about the electronic structure of the coordinated ligand in the UV, visible, and infrared regions. These experimental data are essential for interpreting energy transfer mechanisms in analogous systems containing other Ln^{3+} ions. As shown in Figure S4a, Supporting Information, the in situ emission spectra for LDH-HMA:Gd preparation show only weak broadband in the blue spectral region, extending from 310 to 450 nm ascribed to fluorescence from the $S_1 \rightarrow S_0$ transition of the mellitate anion. It can be highlighted that there is a little Stokes shift among excitation and emission bands indicating that the same ligand states are involved in both absorption and luminescence phenomena (Figure S4b, Supporting Information). Furthermore, both the emission intensity and energy position of the emission band are almost unchanged with the reaction of the metallic salt solution in the reactor. This spectral behavior suggests that intercalated mellitate anions likely experience strong intermolecular interactions in an aqueous solution.[50]

The in situ excitation spectra for LDH-HMA:Ln (Ln: Sm, Eu, Tb and Dy) were recorded by monitoring the intensities of the bands associated with 4f-4f transitions centered on the lanthanide ions: ($^4G_{5/2} \rightarrow {}^6H_{9/2}$, for Sm^{3+}), ($^5D_0 \rightarrow {}^7F_2$, for Eu^{3+}), ($^5D_4 \rightarrow {}^7F_5$, for Tb^{3+}) and ($^4F_{9/2} \rightarrow {}^6F_{11/2}$, for Dy^{3+}). To the best of our knowledge, this is the first time that luminescent properties of LDH-HMA:Ln^{3+} materials containing highly charged aromatic polycarboxylate anion have been monitored in situ processes. Notably, these spectra are dominated by a broad excitation band from the mellitate anion $S_0 \rightarrow S_1$ transition at 305 nm, and the narrow excitation bands with very intensities centered on the lanthanide ions can also be observed (**Figure 4**). In particular, the higher relative intensity of the ligand bands is shown in the excitation spectra for both Zn_2Al- LDH-HMA:Eu and LDH-HMA:Tb materials. This finding indicates that the mellitate ligand is an efficient luminescence sensitizer for Eu^{3+} and Tb^{3+} ions in the LDH material. As can be observed in the inserted photos (Figure 4), under excitation with LED radiation at 310 nm, these samples exhibit very intense red and green luminescence intensities, respectively.

On the other hand, analogous systems containing Sm^{3+} and Dy^{3+} ions display blue and yellow-bluish emissions instead of orange and yellow luminescence colors characteristic of these Ln^{3+} ions, respectively. Although the excitation spectra also show a higher relative intensity for the ligand band ≈300 nm, this result may also reflect the contributions of the blue emission from the ligand. The additional band that appears in the higher energy region in the excitation spectra of these ions also corroborates this statement.

The emission spectra for Zn_2Al-LDH:Ln materials (Ln^{3+}: Eu and Tb) recorded under in situ conditions (**Figure 5**) upon excitation in the $S_0 \rightarrow S_1$ transition (at 305 nm) show only characteristic bands arising from electronic transitions of the Eu^{3+} ($^5D_0 \rightarrow {}^7F_J$) and Tb^{3+} ($^5D_4 \rightarrow {}^7F_J$) ions, where J = 0, 1, 2, 3, 4, 5 and 6. The emission intensities of the $^5D_0 \rightarrow {}^7F_2$ (at 615 nm) and $^5D_4 \rightarrow {}^7F_5$ (at 544 nm) transitions have been monitored as a function of the added volume of salt solution into the reactor. The increase in the emission intensity reinforces that there is an efficient luminescence sensitization of the Eu^{3+} and Tb^{3+} ions by the mellitate anion (Figure S5, Supporting Information). It can be noticed that the emission bands are significantly broadened, indicating the non-heterogeneity of lanthanide sites in the material. In fact, the coordination numbers of the lanthanide ions are higher than those of Zn^{2+} and Al^{3+} ions, so their first coordination sphere on the surfaces of the Zn_2Al-LDH:Ln layers may be completed with water molecules or oxygen atoms from the MA ligand. In the emission spectra for Zn_2Al-LDH:Eu (Figure 5), the band assigned to the $^5D_0 \rightarrow {}^7F_2$ transition is the most prominent, indicating that Ln^{3+} is in a chemical environment without an inversion center. In addition, a single weak band attributed to the $^5D_0 \rightarrow {}^7F_0$ (579 nm) transition is consistent with either C_n or C_{nv} group point. The prominent band at 550 nm assigned to the $^5D_4 \rightarrow {}^7F_5$ transition of the LDH-Tb system reflects its green emission color.

There are no substantial changes in the spectral emission profiles of the Zn_2Al-LDH:Ln materials throughout the reaction for in situ experiments in the function of volume, except for the formation sample with europium ion. It is noteworthy that the emission bands come from the non-degenerate $^5D_0$ emitting level making the Eu^{3+} ion a luminescent probe. Therefore, it exhibits higher sensitivity to slight changes in the chemical environment around the metal ion.

As shown in Figure 5, at the beginning of the reaction in situ, the emission bands from $^5D_0 \rightarrow {}^7F_J$ transitions (J = 0, 1, 2, 3, and 4) of the Eu^{3+} ion show very low intensities and without well-defined splits. However, their spectral profile changes, becoming more noticeable after adding 0.75 mL of the salt solution to the

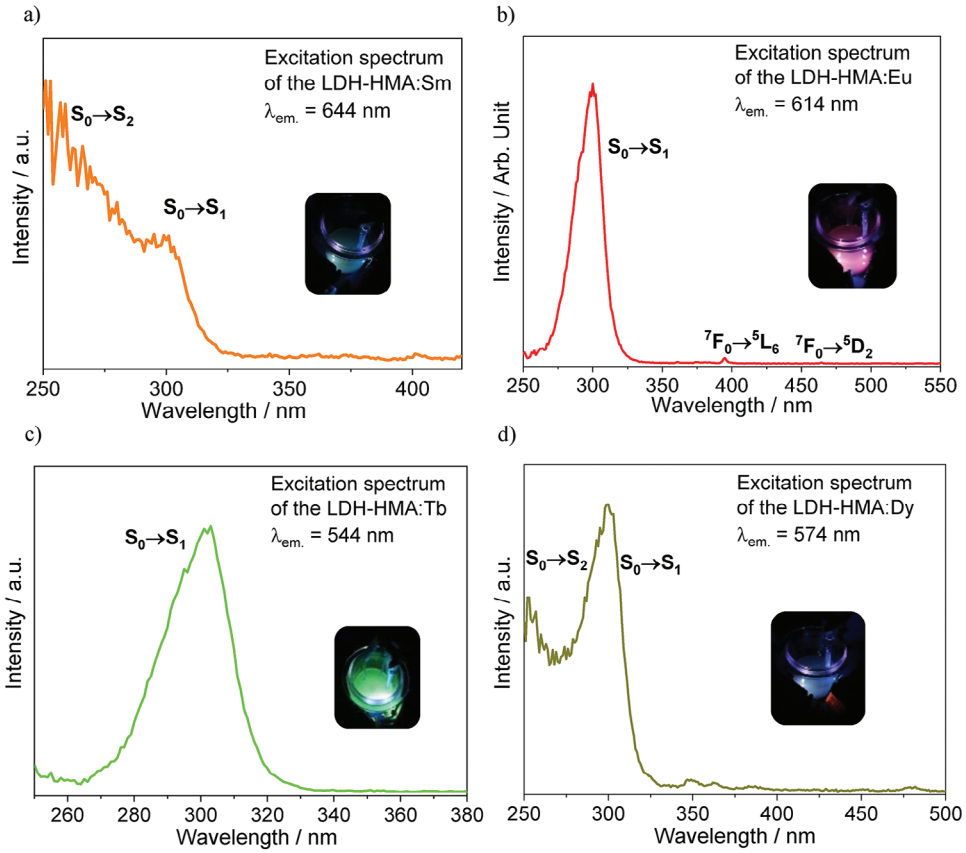

Figure 4. The excitation spectra of the LDH-HMA:Ln materials a) Sm, b) Eu, c) Tb and d) Dy measured in situ upon emission in the 4f-4f transitions. The inserted photographs illustrate the luminescent material colors taken with a digital camera, under LED radiation at 310 nm.

reactor, which corroborates with a significant increase in light scattering measurements in the same reaction step (Figure 2). This finding suggests an increase in the concentration of the nucleation followed by the particle growth processes.[35] The change in spectral behavior is best observed by comparing the emission spectra recorded after the addition of 0.17 and 3.33 mL of the salt solution into the reactor (Figure S6, Supporting Information). A similar optical behavior is observed in the emission spectra for the LDH-HMA:Tb, but lowly pronounced. Therefore, it is possible to confirm that the growth process induces changes in the lanthanide chemical environment, reflected in the different emission spectral profiles of the Eu^{3+} and Tb^{3+} systems.

To better explore the changes in the luminescence properties with the particle growth of the LDH-HMA:Eu material, the experimental intensity parameters Ω_2 and Ω_4 were determined from the emission spectral data as described in the literature.[51]

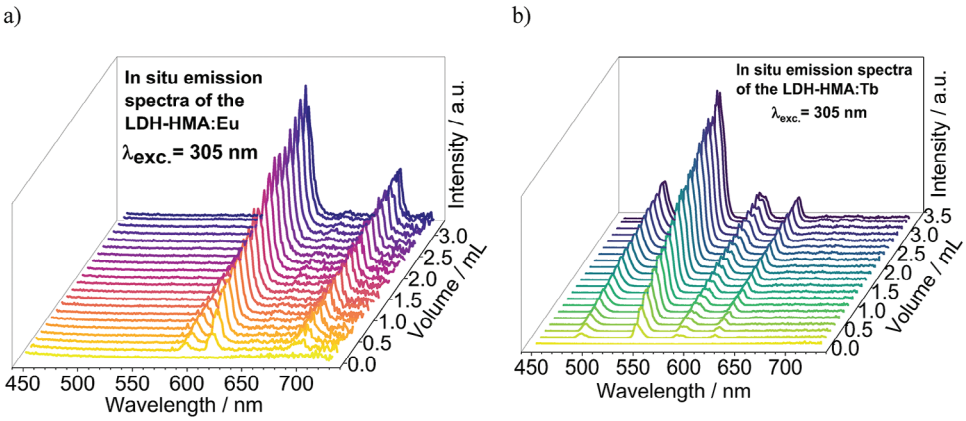

Figure 5. a) The emission spectra of the LDH-HMA:Eu and LDH-HMA:Tb materials measured in situ upon excitation in the mellitate $S_0 \rightarrow S_1$ transition at 305 nm.

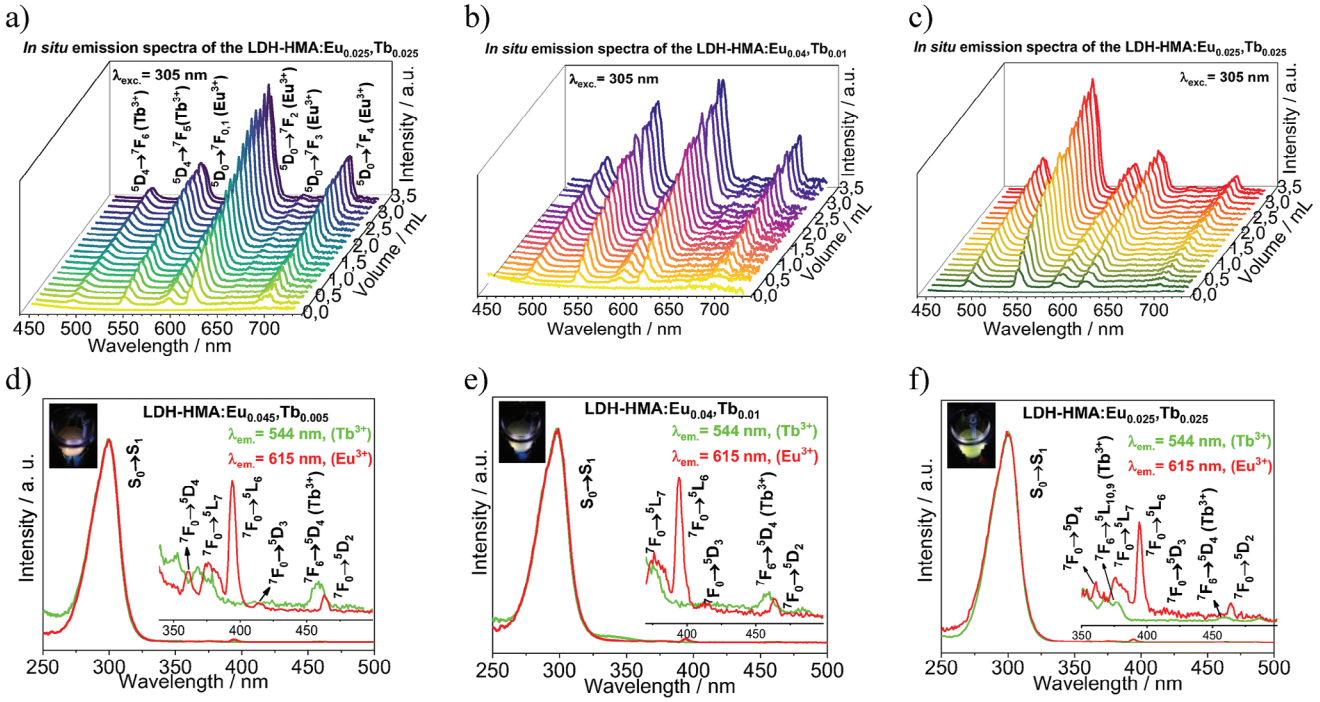

Figure 6. The emission spectra of the LDH-HMA:$Eu_{0.05-x}$,Tb_x materials (a: x = 0.005, b: x = 0.01 and c: x = 0.025) measured in situ upon excitation in the mellitate $S_0 \rightarrow S_1$ transition at 305 nm. The excitation spectra of the LDH-HMA:$Eu_{0.05-x}$,Tb_x materials measured in situ with emission monitored in the intraconfigurational transitions of the lanthanide ions (d: x = 0.005, e: x = 0.01 and f: x = 0.025).

Figure S7a, Supporting Information shows that the most pronounced changes in the Ω_2 value occur between additions of 0.17 and 0.75 mL of salt solution, increasing from 4.2×10^{-20} cm^2 to 5.6×10^{-20} cm^2. With the addition of more salt solution, fluctuations in the value of this parameter are observed without significant angular changes, which is consistent with the growth of LDH particles after nucleation. The smaller changes in the Ω_4 parameter values (Figure S7b, Supporting Information) suggest a minor variation in ligand-metal distances in LDH-HMA:Ln^{3+} materials.[22]

The emission spectra of the LDH-HMA:Sm^{3+} recorded in the spectral range of 500 to 720 nm reveal narrow bands attributed to the $^5G_{5/2} \rightarrow {}^6H_J$, where J = 5/2 (560 nm), 7/2 (597 nm) and 9/2 (643 nm) as shown in Figure S8a, Supporting Information. A broad emission band in the low wavelength spectral region is also observed due to mellitate anion emission, which is owing to a less efficient ligand-to-metal energy transfer process (Figure S8, Supporting Information). Although the emission band due to the hypertensive $^5G_{5/2} \rightarrow {}^6H_{9/2}$ transition is the prominent one, its intensity is almost comparable to the emission of the ligand. In addition to the low efficiency in the energy transfer between the mellitate anion and the Sm^{3+} ion, non-radiative decay processes are quite efficient, contributing to the emission intensities due to the intraconfigurational transitions. Besides, the in situ emission spectra for LDH-HMA:Dy^{3+} systems display the narrow bands arising from the $^4F_{9/2}$ emitting levels (Figure S8b, Supporting Information): $^4F_{9/2} \rightarrow {}^6H_{15/2}$ (480 nm), $^4F_{9/2} \rightarrow {}^6H_{13/2}$ (575 nm), and $^4F_{9/2} \rightarrow {}^6H_{11/2}$ (665 nm). Similar to that observed for the Sm^{3+} system, a broad emission band from the intercalated mellitate anion also appears in the higher energy region. However, the relative emission intensity due to the intraconfigurational $^4F_{9/2} \rightarrow {}^6H_{13/2}$ transition is significantly higher than those in the emission spectra of the Zn_2Al-LDH:Sm^{3+} material, suggesting that the luminescence sensitization process is more efficient in the LDH-Dy^{3+} than in the analogous Sm^{3+} material. Therefore, in contrast to the LDH-HMA:Sm^{3+}, the emission color of the Dy^{3+} system is closer to the characteristic yellow color.

In situ luminescence was also carried out for LDH-HMA:$Eu_{0.05-x}$:Tb_x, where x = 0.005, 0.01, and 0.025, which correspond to the molar percentage Tb/Eu ratios of 10, 20 and 50%, respectively. As demonstrated in **Figure 6**, for all investigated Eu/Tb ratios, the emission spectra upon excitation at 305 nm present the characteristic bands from intraconfigurational transitions of both Eu^{3+} ($^5D_0 \rightarrow {}^7F_J$) and Tb^{3+} ($^5D_4 \rightarrow {}^7F_J$) ions. In addition, the spectral profiles of these bands are similar to those for LDH-HMA:Eu and LDH-HMA:Tb materials that contain only Eu^{3+} or Tb^{3+} ions, respectively. This is an expected result since these metal ions produce isomorphous materials. However, the increase in the amount of Tb^{3+} ion results in a sudden increase in the relative intensities of the bands of this metal ion (Figure S9, Supporting Information). For example, even for the ratio Tb^{3+}/Eu^{3+} equal to 20% (x = 0.005), the emission bands due to the $^5D_4 \rightarrow {}^7F_5$ (Tb^{3+}) and $^5D_0 \rightarrow {}^7F_2$ (Eu^{3+}) transitions present similar relative intensities (Figure 6b). In particular, for Tb^{3+}/Eu^{3+} ratio of 50%, the first band $^5D_4 \rightarrow {}^7F_5$ (Tb^{3+}) is the dominant one (Figure 6c). This result indicates that the mellitate anion acts as a more efficient luminescence sensitizer for Tb^{3+} than Eu^{3+} ion in the in situ conditions of LDH-HMA:Ln formation.

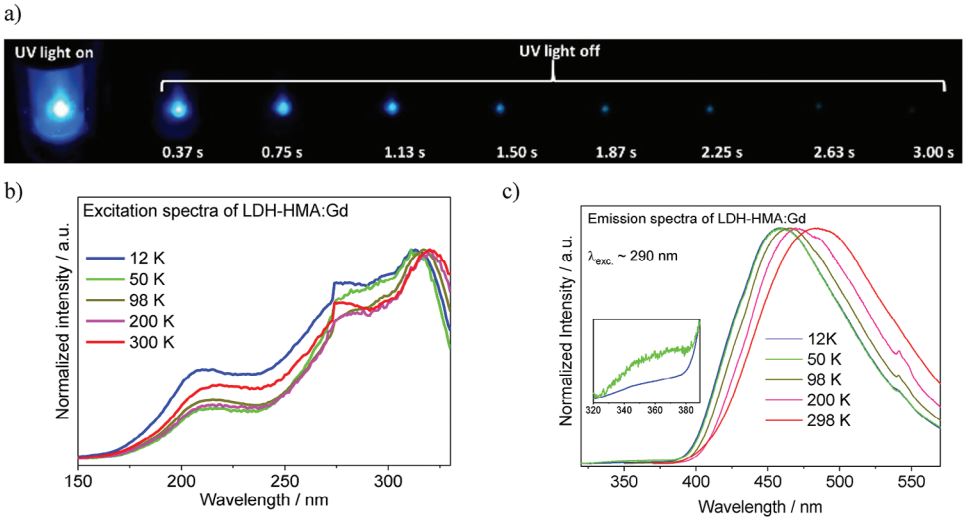

Figure 7. a) Luminescence of the LDH-HMA:Gd sample containing mellitate anion under irradiation with UV light (left) at 310 nm and up to 3 s after the UV light source was turned off. b) Excitation spectra of the Zn_2Al-LDH:Gd sample containing mellitate anion recorded at different temperatures with emission monitored at 460 nm and c) Emission spectra of the LDH-HMA:Gd sample containing mellitate anion recorded at different temperatures under excitation at 310 nm.

To investigate the possibility of energy transfer between lanthanide ions, excitation spectra were recorded by selective monitoring emission intensities of the bands due to the $^5D_4 \rightarrow {}^7F_5$ (Tb^{3+}, at 542 nm) and $^5D_0 \rightarrow {}^7F_2$ (Eu^{3+}, at 616 nm) transitions. As can be observed in Figure 6d–f, only a broad intense band ≈305 nm is assigned to the $S_1 \rightarrow S_0$ transition from mellitate anion and narrow bands due to 4f-4f transitions centered on the lanthanide ion. Although non-radiative $Tb^{3+} \rightarrow Eu^{3+}$ energy transfer processes are very common in different kinds of materials doped with these cations,[52,53] the absence of bands from the Tb^{3+} ion in the excitation spectra obtained under emission at the $^5D_0 \rightarrow {}^7F_2$ (Eu^{3+}, at 616 nm) transition strongly reinforced the X-ray diffraction data that there is no formation of lanthanide mellitate metal-organic frameworks in the reactor during the LDH-HMA:Ln preparation process. It is worth mentioning that the shortest intermetallic distance Ln^{3+}-Ln^{3+}in MOFs with the mellitate ion is ≈5.9 angstroms,[54] which should result an efficient energy transfer $Tb^{3+} \rightarrow Eu^{3+}$ in the case of the formation of a polymeric coordination compound.

3.1.2. Ex Situ Luminescence Investigation

The photophysical properties of the mellitate anion in LDH-HMA:Ln after filtering, washing, and drying at 60 °C were investigated based on the emission and excitation spectral data, as well as the luminescence decay curves. Although the mellitate organic anion absorption is not significantly affected by the type of lanthanide ion, the photophysical properties of the LDH-HMA:Ln largely depend on the energy transfer mechanisms from the ligand to the central metal ion. Surprisingly, the LDH-HMA:Gd material exhibited unusually high intense greenish-blue luminescence at room and low temperatures. This spectroscopic behavior makes the LDH-HMA:Gd material a potential candidate for applications in afterglow LEDs, sensing, anti-counterfeiting, and bioimaging.[55,56] Moreover, even after turning off the excitation source at 310 nm, it displays a remarkable afterglow emission, lasting for a few seconds by the naked eye (**Figure 7a**, Movie S1, Supporting Information). To survey the origin of this phenomenon, steady-state and time-resolved luminescent spectra were recorded at different temperatures. As shown in Figure 7b, the excitation spectra recorded in the vacuum-ultraviolet wavelength regions from 150 to 330 nm with emission monitored at 450 nm exhibit three overlap absorption bands, which can be assigned to $S_0 \rightarrow S_1$ (≈310 nm), $S_0 \rightarrow S_2$ (≈270 nm) and $S_0 \rightarrow S_3$ (≈220 nm) transitions of the mellitate anion. As can be observed in Figure S4, Supporting Information, only the excitation band at a higher wavelength is presented for in situ measurement for this sample. The energy positions of these bands at higher energies are practically not shifted by temperature variation, except the band from the $S_0 \rightarrow S_1$ transition shows a slight shift toward longer wavelengths with increasing temperature.

Figure 7c displays the steady-state emission spectra recorded at different temperatures in the 320 to 600 nm range upon excitation at 300 nm. These spectra reveal overlapped broad emission bands from 400 to 570 nm, which are considerably shifted compared to the absorption bands. Consequently, they can be assigned to the phosphorescence $T \rightarrow S_0$ transitions from the mellitate ligand, probably due to the molecular structure rigidity of the organic anion. Similar behavior was also observed for Gd-mellitate metal-organic frameworks.[57] It should be noted that the shoulder in the higher energy region decreases its intensity with increasing temperature. This result suggests that different emitting states contribute to emission, reflecting the non-homogeneity of the organic anions between layers of LDHs. It is worth mentioning that mellitate anions may interact differently with the other chemical species of LDHs, showing slightly different spectroscopic properties. This fact is associated with conformational changes of the HMA^{-5} anion with increasing temperature, which may contribute to the observed shift of the emission band maximum to longer wavelengths. Under magnification of the spectral scale (inset in Figure 7b), it is also possible

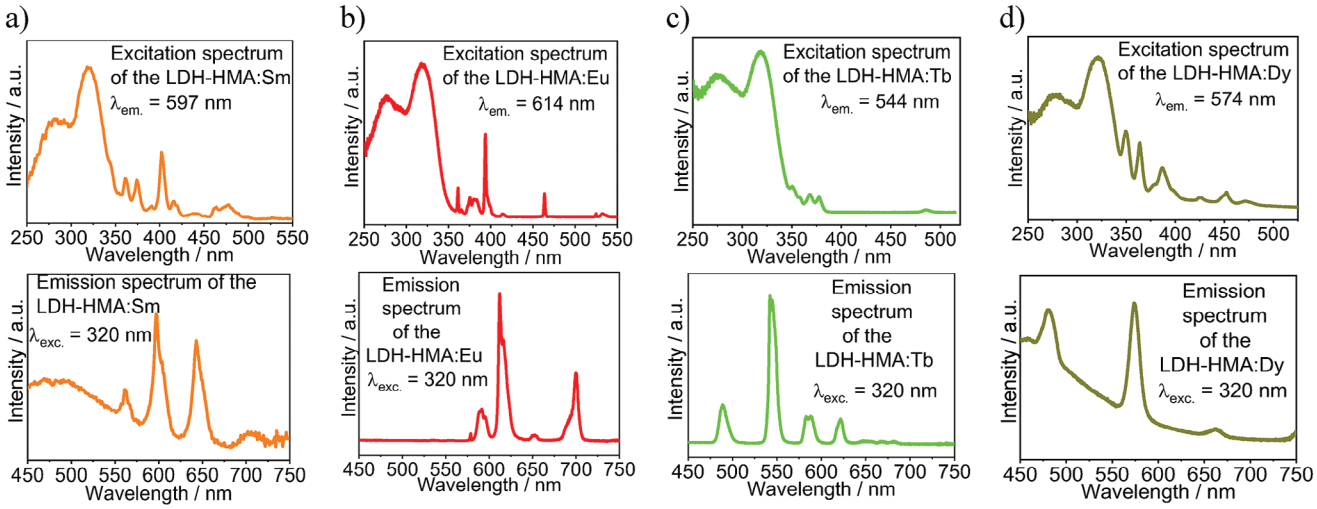

Figure 8. Excitation and emission spectra for LDH-HMA:Ln materials recorded under ex situ conditions with emission monitored on the more intense intraconfigurational transition of the Ln^{3+} ion and upon excitation at 320 nm corresponding to the $S_0 \rightarrow S_1$ transition of the mellitate anion.

to observe a fluorescence band in a similar spectral region as in situ measurements; however, it exhibits a very low relative intensity. The reason why aromatic carboxylates intercalated into interlayered inorganic materials exhibit afterglow phosphorescence is still a topic of wide discussion in the literature.[20] However, intermolecular interactions that limit intramolecular motions and, therefore, minimize non-radiative processes involving the excited triplet state, as well as n-π^* transitions of the carboxylate moieties that contribute to enhancing the spin-orbit coupling seem to play the most important role of this intriguing spectroscopic phenomenon. It is worth mentioning that the emission spectrum of mellitic acid in the solid state was also recorded (Figure S10a, Supporting Information), showing only a broad fluorescence band in the 450 nm region attributed to the $S_1 \rightarrow S_0$ transition of this acid. This result was confirmed by the short average lifetime value ($\tau = 3.0$ ns) obtained from the luminescence decay curve of mellitic acid (Figure S10b, Supporting Information). This behavior indicates that the afterglow phenomenon is characteristic of the mellitic ion intercalated in the inorganic material.

The luminescence decay curves of material LDH-HMA:Gd recorded at 298 and 77 K temperatures are consistent with the observed afterglow behavior. These curves demonstrate significantly slow bi-exponential decays, presenting shorter and longer lifetimes of milliseconds, 1.5 and 12 ms at 298 K and 5.0 ms and 18 ms at 77 K (Figure S11, Supporting Information).

Interestingly, the ex situ excitation spectra for the LDH-HMA:Ln (Ln: Sm, Eu, Tb and Dy) systems recorded at room temperature from 250 to visible spectral region are shown in **Figure 8**. As also observed for in situ experiments, these data revealed that the same ligand excited states are involved in the photophysical processes in the LDH-HMA:Ln materials. These spectra were recorded with emission monitored on the intraconfigurational transitions of the lanthanide ions: ($^4G_{5/2} \rightarrow {}^6H_{9/2}$, for Sm^{3+}), ($^5D_0 \rightarrow {}^7F_2$, for Eu^{3+}), ($^5D_4 \rightarrow {}^7F_5$, for Tb^{3+}) and ($^4F_{9/2} \rightarrow {}^6F_{11/2}$, for Dy^{3+}). Comparing data with those for in situ measurements, two main differences in the spectral profiles are observed. First, an additional broad band with a maximum of ≈270 nm ascribed to the mellitate $S_0 \rightarrow S_2$ transition can be observed. Second, the relative intensities of the narrow bands due to the 4f-4f transitions: ($^4G_{5/2} \rightarrow {}^6H_{9/2}$, Sm^{3+}), ($^5D_0 \rightarrow {}^7F_2$, Eu^{3+}), ($^5D_4 \rightarrow {}^7F_5$, Tb^{3+}) and ($^4F_{9/2} \rightarrow {}^6F_{11/2}$, Dy^{3+}) are higher in the ex situ excitation spectra. These data reflect a slight decrease in the efficiency of the lanthanide luminescence sensitization processes for the LDH-HMA:Ln after thermal treatment at 60 °C. This result is in line with X-ray data for a short basal distance in these LDHs, which suggests that the mellitate anion probably undergoes reorganization between the LDHs layers after the drying process and, consequently, changes its form of interaction with the metallic ions. However, an efficient energy transfer can still occur from the sensitizer in the interlamellar region to the Ln^{3+} ion in LDH. As observed in Figure 8b, the broad bands arising from the mellitate are prominent in excitation spectra. In particular, for the LDH-Tb system (Figure 8c), the relative intensity of the organic anion bands is exceptionally high, indicating that energy transfer is quite efficient in this case. This result is in good agreement with Latva's rule.[58]

It is important to mention the energy transfer processes from mellitate anion to Eu^{3+} and Tb^{3+} ions are very efficient due to the quasi-resonant conditions among triplet excited state of the energy donor (mellitate) and the excited $^{2S+1}L_J$ energy levels of these acceptor Ln^{3+} cations. Therefore, the phosphorescence band assigned to the $T_1 \rightarrow S_0$ transition of the mellitate is efficiently quenched by the lanthanide ions. This optical feature leads to highly red and green luminescent materials from Eu^{3+} and Tb^3 ions (Figure 8b,c), respectively. On the other hand, the lowest excited level ($^6P_{7/2}$) of the Gd^{3+} ion has exceptionally high energy (≈32 000 cm^{-1}) as compared with the excited T_1 states of most organic ligands. In this case, the energy transfer involving the triplet state and the first excited $^6P_{7/2}$ level of the Gd^{3+} ion is poorly operative, resulting in a room temperature phosphorescence ($T \rightarrow S_0$) centered on the organic anion (Figure 7c).

The emission spectra of LDH-HMA:Eu and LDH-HMA:Tb materials recorded at room temperature in the range of 450–720 nm upon excitation at 310 nm (Figure 8f,g) show the typical narrow bands corresponding to the $^5D_0 \rightarrow {}^7F_J$ (Eu^{3+}, J = 0–4) and

$^5D_4 \rightarrow {}^7F_J$ (Tb^{3+}, J = 0–6) transitions. The absence of the phosphorescence band from the mellitate anion indicates that an efficient luminescence sensitization of the Ln^{3+} ions also occurs in dried materials with Eu^{3+} and Tb^{3+} ions. As mentioned, the ligand donor triplet state (T_1) is in the most appropriate relative position to transfer energy to the Tb^{3+} ion. Quantitative analyses of the spectral data were also performed ex situ for the LDH-HMA:Eu material from the intensity Ω_2 and Ω_4 parameters. It is worth noting that the $\Omega_2 = 6.45\times10^{-20}$ cm^2 and $\Omega_4 = 6.24\times10^{-20}$ cm^2 values are higher than those determined from in situ spectral data, which can be assigned to the slight structural changes in the chemical environment of Eu^{3+} ion after washing, and drying sample at 60 °C. However, the higher changes occurred in the Ω_2 value, indicating that angular changes are more pronounced with the drying process. It is worth mentioning that the luminescence decay curve for the LDH-HMA:Eu system recorded upon excitation on the ligand band (at 310 nm) and emission monitored on the $^5D_0 \rightarrow {}^7F_2$ transition of Eu^{3+} ion adjusted well to a single exponential function, resulting in a low lifetime (τ) value for the $^5D_0$ emitting level equal to 0.2421 ms (Figure S12, Supporting Information). This result indicates that Eu^{3+} ions in the LDH are found in similar chemical environments. Furthermore, radiative (A_{rad} = 342 s^{-1}) and non-radiative (A_{nrad} = 4130 s^{-1}) rates were also determined from the procedure described in reference.[22] The latter was obtained from the relation [$A_{nrad} = 1/(\tau - A_{rad})$]. The high value of A_{nrad} is consistent with the luminescence quenching effect due to the OH groups coordinated to the Eu^{3+} ion that resulted in a low intrinsic quantum yield value ($Q^{Eu}_{Eu} = A_{rad}.\tau$ x 100 = 8.2%) for the LDH-HMA:Eu material.

Analogously to that observed for in situ emission spectra of the LDH-HMA:Sm and LDH-HMA:Dy samples (Figure 8e,h), their ex situ spectra also showed the bands due to these intraconfigurational transitions of the Sm^{3+} $^5G_{5/2} \rightarrow {}^6H_J$, where J = 5/2 (560 nm), 7/2 (598 nm) and 9/2 (644 nm) and Dy^{3+} $^4F_{9/2} \rightarrow {}^6H_{15/2}$ (480 nm), $^4F_{9/2} \rightarrow {}^6H_{13/2}$ (574 nm), and $^4F_{9/2} \rightarrow {}^6H_{11/2}$ (665 nm). As can be seen, the broadband in the 460 nm region arising from this transition overlaps more effectively with those attributed to the metal center transitions than for in situ spectra. This behavior arises from the phosphorescence emission of the ligand in the ex situ spectra. While in the LDH-HMA:Sm sample, the ligand bands practically mask the Sm^{3+} bands that reflect a very low transfer of energy from the mellitate anion to this metal ion. On the other hand, the main emission bands of the dysprosium ion in the LDH-HMA:Dy material are observed. Therefore, the energy transfer process from the organic anion to the Dy^{3+} ion is more efficient than that involving the Sm^{3+} ion, as obtained for in situ luminescence data.

The extrinsic quantum yield (Q^L_{Ln}) of the LDH-HMA:Eu and LDH-HMA:Tb samples were also determined with excitation monitored at 310 nm on the mellitate $S_0 \rightarrow S_1$ transition and emission recorded in the spectral interval 420–720 nm at room temperature. As reported above, emission spectra recorded at room temperature do not show the phosphorescence band from the organic ligand. Thus, Q^L_{Ln} values represent the balance between the emission of the metallic center when the lanthanide ion is indirectly excited via energy transfer from the mellitate anion. Despite the high intensity observed for the emission of the LDH-Eu sample, Q^L_{Eu} = 2.3% value is due to a lower sensitization of the mellitate anion and, mainly, as expected due to the multiphonon suppression effect of the OH groups coordinated to the Eu^{3+} ion. On the other hand, the highest value of Q^L_{Tb} = 30% for LDH-Tb corroborates the excitation and emission data. In this case, in addition to the efficient energy transfer from the mellitate anion to the metal center being more efficient, the multiphonon luminescence quenching processes are less effective for the Tb^{3+} ion owing to the high energy gap of Tb^{3+} ion ($^5D_4 \rightarrow {}^7F_0$, ΔE = 14 800 cm^{-1}) compared with that Eu^{3+} ion ($^5D_0 \rightarrow {}^7F_6$, ΔE = 12.000 cm^{-1}). This quenching effect may be supported by the luminescence decay curve behavior for the Zn_2Al-LDH:Tb material recorded upon excitation at 310 nm of mellitate anion and emission monitored on the $^5D_4 \rightarrow {}^7F_5$ transition (at 544 nm). This curve presents a single exponential function, yielding a high τ = 0.838 ms value for the $^5D_4$ emitting level (Figure S12, Supporting Information). On the other hand, the LDH-HMA:Sm and LDH-HMA:Dy samples exhibit smaller lifetime values of their emitting level, $^5G_{5/2}$ (Sm^{3+}) and $^4F_{9/2}$ (Dy^{3+}) (Figure S9, Supporting Information). Again, this behavior reflects the very efficient luminescence quenching processes in these materials. Therefore, the very low emission intensity for the LDH-HMA:Sm and LDH-HMA:Dy samples made it impossible to obtain their extrinsic quantum yield values.

The photostabilities of the LDH-HMA:Tb and LDH-HMA:Eu materials were investigated under radiation at 310 nm for 4h. As can be seen in Figure S13, Supporting Information, no significant changes in emission intensity are observed, indicating that LDH-HMA:Tb material sample may present a high photostability to radiation in the UV region. However, the emission intensity of the LDH-HMA:Eu material decreases ≈30% of the initial value. This behavior can probably be associated with conformational changes of the mellitate anion that can alter the energy structure of the ligand and, consequently, decreasing more significantly the luminescence sensitization of the Eu^{3+} ion by the mellitate anion. However, further investigation to explain this photophysical behavior can be carried out in future work.

The photoluminescent properties of the LDH-HMA:$Eu_{0.05-x}$:Tb_x samples (after drying treatment, ex situ) were also compared with those obtained for in situ experiments. **Figure 9a** shows the excitation spectra for the LDH-HMA:$Eu_{0.025}$:$Tb_{0.025}$ sample recorded at room temperature from 250to 450 and 250 to 590 nm under emission monitored on the $^5D_4 \rightarrow {}^7F_5$ (Tb^{3+}, 542 nm) and $^5D_0 \rightarrow {}^7F_2$ (Eu^{3+}, 616 nm) transitions, respectively. As can be observed, these spectra display an increase in the relative intensity of the narrow absorption bands from the intraconfigurational-4f transitions, as compared with in situ experiments (Figure 6). Even after drying and in the molar Eu^{3+}/Tb^{3+} ratio equal to 1, absorption bands from the Tb^{3+} ion exhibit only very low intensity in the excitation spectrum when the emission is monitored in the Eu^{3+} ion. In this case, it can be stated that there is no formation of coordination polymers and that the lanthanide ions are far from each other, which minimizes the possibility of energy transfer between them.

The ex situ emission spectra for the LDH-HMA:$Eu_{0.05-x}$,Tb_x samples recorded under excitation at 320 nm of the mellitate $S_0 \rightarrow S_1$ transition is depicted in Figure 9b. It is worth noting that the relative intensities among emission bands from the $^5D_4 \rightarrow {}^7F_J$ (for Tb^{3+} ion) and $^5D_0 \rightarrow {}^7F_J$ (for Eu^{3+} ion) transitions also become higher when the molar ratio of the Tb^{3+} ion in the LDHs is increased. However, this optical is less noticeable than that revealed

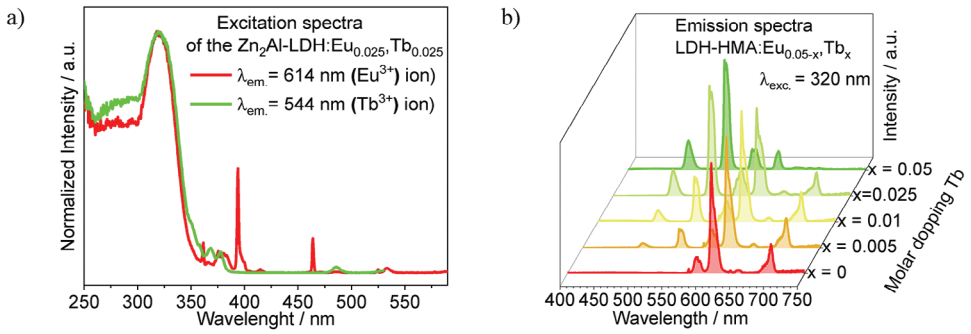

Figure 9. a) Excitation and emission spectra for the Zn_2Al-LDH:$Eu_{0.025}$:$Tb_{0.025}$ material recorded *ex situ* conditions with emission selectively monitored on the from the $^5D_4 \rightarrow {}^7F_J$ (for Tb^{3+} ion) and $^5D_0 \rightarrow {}^7F_J$ (for Eu^{3+} ion) transitions. b) Emission spectra for the Zn_2Al-LDH:Eu_{1-x}:Tb_x material (x = 0, 0.005, 0.010, 0.025 and 0.05) upon excitation at 320 nm corresponding to the $S_0 \rightarrow S_1$ transition of the mellitate anion.

by the in situ analyses (Figure 6). For example, while the in situ emission spectrum of the LDH-HMA:$Eu_{0.025}$,$Tb_{0.025}$ sample is dominated by the band assigned to the $^5D_4 \rightarrow {}^7F_5$($Tb^{3+}$) transition, the ex situ emission spectrum (Figure 9b) reveals this band is only slightly more intense than that one from the $^5D_0 \rightarrow {}^7F_2$($Eu^{3+}$) transition. Some points can be highlighted to justify this spectral behavior. First, drying the material can significantly reduce the degree of hydration of the metal centers in the LDH, reducing luminescence quenching effects. Second, dehydration can increase the amount of lanthanide ions coordinated by the mellitate anion and shorten this interaction. In this case, energy transfer from the ligand to the lanthanide ion may be significantly improved.

CIE colour coordinates (x,y) for the LDH-HMA:Ln determined based on the in situ and ex situ luminescence data are shown in **Figure 10**. For both in situ and ex situ experiments, LDH-HMA:Eu and Zn_2Al-LDH:Tb displayed characteristic red and green luminescence colors due to the most prominent bands from $^5D_4 \rightarrow {}^7F_J$ (Tb^{3+}) and $^5D_0 \rightarrow {}^7F_J$ (Eu^{3+}) transitions. Overall, the color coordinates shift toward the green region with increasing Tb^{3+} ion doping concentration (Figure 10a), which agrees with the higher extrinsic quantum yield determined for

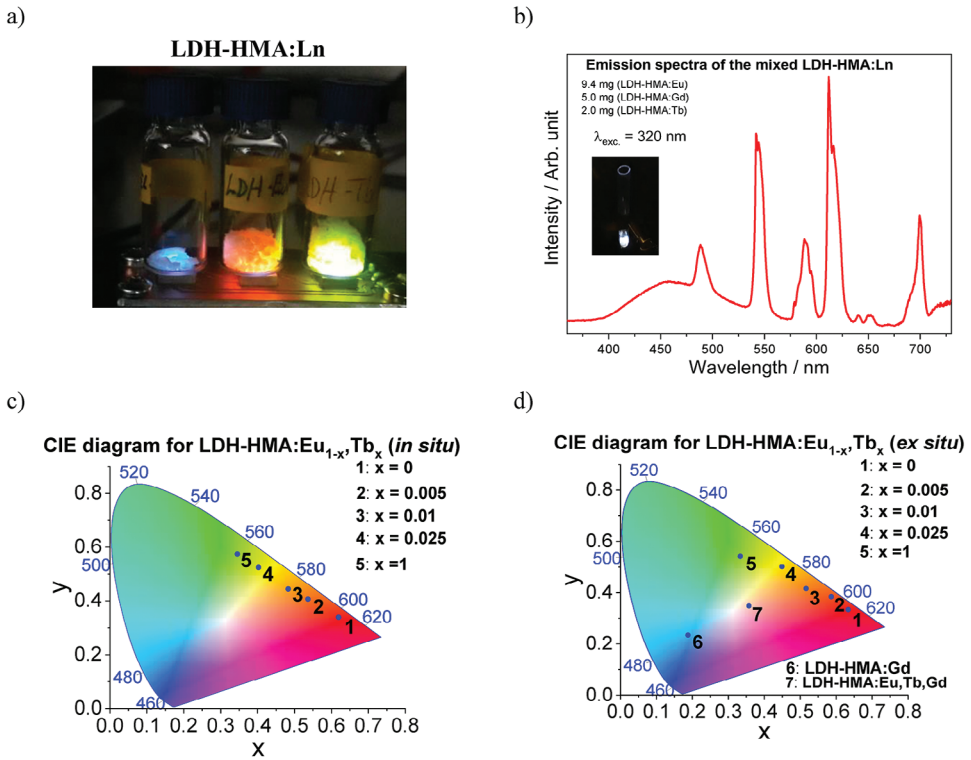

Figure 10. a) Photograph illustrating the luminescent material colors taken with a digital camera, under LED radiation at 310 nm. b) Emission spectrum of the mixed LDH-HMA:Ln materials (Ln: Eu, Gd and Tb), containing 9.4 (LDH-HMA:Eu), 5.0 (LDH-HMA:Gd), and 2.0 mg (LDH-HMA:Tb). Chromaticity diagrams CIE-xy for the LDH-HMA:Ln materials based on the emission spectra recorded c) in situ and d) ex situ upon excitation at 320 nm corresponding to the $S_0 \rightarrow S_1$ transition of the mellitate anion. The CIE coordinate of the mixed LDH-HMA:Ln materials (Ln: Eu, Gd and Tb) (point 7: LDH-HMA:Eu,Tb,Gd).

the LDH-HMA:Tb. However, this effect is less pronounced for ex situ experiments (Figure 10b), corroborating the decrease in the efficiency due to Eu^{3+} ion luminescence quenching effect.

Owing to the high phosphorescence intensity of the LDH-HMA:Gd system in the blue region, its color coordinate was also determined from the emission spectrum recorded at room temperature. As shown in Figure 10b, the broad emission band with a maximum at 460 nm yield is more shifted toward a blue-greenish material with color coordinates (0.1879, 0.2344) far from the diagram's vertex. However, taking advantage of the high red, green and blue emission intensities of LDHs doped with Eu^{3+}, Tb^{3+} and Gd^{3+} ions, respectively, it was possible to obtain a mixed LDH-HMA:Ln material containing 9.4 mg (LDH-HMA:Eu), 5.0 mg (LDH-HMA:Gd) and 2.0 mg (LDH-HMA:Tb) with a color coordinate close to the white region (0.35749, 0.34771) (Figure 10b and Movie S2, Supporting Information). The photoluminescence quantum yield value (PLQY = 6.5%) of the white light phosphor was also determined, which reflects the lowest yield value of the LDH-HMA:Eu material. Although white light-emitting materials with yield values above 20% are found in the literature, the high luminescence intensity presented by LDH-HMA:Ln (Eu^{3+}, Gd^{3+}, and Tb^{3+}) can act as promising for photonic applications.[55,56] This result indicates that LDH-HMA:Ln materials containing the mellitate anion as a luminescence sensitizer are promising phosphors for the development of white-emitting devices under excitation at the UV region.

4. Conclusions

In summary, we demonstrate the feasibility to prepare Ln^{3+} doped LDHs intercalated with highly negative carboxylate anion by co-precipitation method. Infrared spectroscopy, elemental analysis, and thermogravimetry data suggest the general chemical formula $[Zn_2Al_{0.95}:Ln_{0.05}(OH)_6](HMA)_{0.21}\cdot(H_2O)_x$, where x = 1.0–1.7 and Ln^{3+}: Sm^{3+}, Eu^{3+}, Gd^{3+}, Tb^{3+} and Dy^{3+}, in which the intercalated mellitate anion is HMA^{-5} rather than the fully ionized species MA^{-6}. Taking into account the in situ data, we have demonstrated that the luminescence properties of the Eu^{3+} may be investigated to monitor slight structural changes during the formation of LDH systems. A comparison between in situ and ex situ measurements reveals significant changes in the photophysical properties with the drying treatment of the samples, which may be assigned to the reorganization of the mellitate anion in the structure of the materials. The X-ray diffraction data of the materials agree with this proposal. Even in the interlayer gallery of the LDH, mellitate anion act as an efficient luminescence sensitizer for Eu^{3+} and Tb^{3+} ions, generating highly luminescent LDH-HMA:Eu^{3+} and LDH-HMA:Tb^{3+} materials. In particular, the highest extrinsic quantum yield (Q_{Ln}^{L} = 30%) found for the Tb^{3+} sample is consistent with an operative antenna effect. Despite the low Q_{Ln}^{L} value for the LDH-HMA:Eu^{3+} material due to the high non-radiative decay rate caused by the multiphonon relaxation process, this material still presents high luminescence intensity. The high luminescence intensities in the red, green, and blue spectral regions for LDHs doped with Eu^{3+}, Tb^{3+}, and Gd^{3+} ions, respectively, offer a simple pathway to obtain rich tunable multicolor and white-light emission materials for lighting devices.

Supporting Information

Supporting Information is available from the Wiley Online Library or from the author.

Acknowledgements

The authors thank the German Research Foundation's (DFG) priority Program 1415, the German Academic Exchange Service (DAAD), the Coordination for the Improvement of Higher Education Personnel "CAPES" for their financial support. Parts of this research were carried out at PETRA III at DESY, a member of the Helmholtz Association (HGF). The authors acknowledge DESY (Hamburg, Germany), a member of the Helmholtz Association HGF, for the provision of experimental facilities. Parts of this research were carried out at PETRA III beamline P66 (proposal ID I-20220438). D.M., H.F.B., and I.F.C. acknowledge Fundação de Amparo à Pesquisa do Estado de São Paulo (FAPESP, grants 2022/01314-8, 2022/12709-3 and 2021/08111-2), CNPQ 308872/2022-3 and Coordenação de Aperfeiçoamento de Pessoal de Nível Superior (CAPES, grant 88887.371434/2019-00) for financial support. E.E.S.T. also thank to CAPES (CAPES, grant 88887.647236/2021-00) and Universidade Federal da Paraíba (UFPB) for financial support.

Open access funding enabled and organized by Projekt DEAL.

Conflict of Interest

The authors declare no conflict of interest.

Author Contributions

E.E.S.T.: Conceptualization, Methodology, Investigation, Formal Analysis, Data Curation, Validation, Visualization, Writing – Original Draft, Writing – Review & Editing. **G.D.**: Conceptualization, Methodology, Investigation, Formal Analysis, Data Curation, Validation, Visualization, Writing – Original Draft, Writing – Review & Editing. **J.S,**: Visualization, Data curation, Investigation, Writing – Review & Editing. **D.M,**: Conceptualization, Methodology, Resources, Supervision, Writing – review & editing. **A.K,**: Conceptualization, Methodology, Resources, Supervision, Writing – review & editing. in-**H.T.**: Resources, Supervision, Writing – review & editing. **I.F.C.**: Formal Analysis, Data Curation, Validation, Visualization, Writing – Review & Editing. **H.F.B.**: Data curation, Investigation, Writing – original draft.

Data Availability Statement

The data that support the findings of this study are available from the corresponding author upon reasonable request.

Keywords

in situ and ex situ luminescence, lanthanide ions, layered double hydroxides, mellitate anion, white-light emission

Received: August 14, 2024
Revised: October 7, 2024
Published online: November 2, 2024

[1] T. Selvam, A. Inayat, E. Schwieger, *Dalton Trans.* **2014**, *43*, 10365.
[2] B. R. Gevers, E. Roduner, F. J. W. J. Labuschagné, *Mater. Adv.* **2022**, *3*, 962.

[3] A. V. Radha, S. Weiß, I. Sanjuán, M. Ert, C. Andronescu, J. Breu, *Chem. - Eur. J.* **2021**, *27*, 16930.
[4] M. Kiani, M. Bagherzadeh, A. M. Ghadiri, P. Makvandi, N. Rabiee, *Sci. Rep.* **2022**, *12*, 9461.
[5] K. Zeng, M. Tian, X. chen, J. Zhang, M. H. Rummeli, P. Strasser, J. Sun, R. Yang, *Chem. Eng. J.* **2023**, *452*, 139151.
[6] C. I. Lisevski, A. F. Morais, N. F. Aguero, A. C. Teixeira, F. W. M. Ribeiro, T. C. Correra, I. G. N. Silva, D. Mustafa, *ACS Omega* **2024**, *9*, 32962.
[7] A. F. Morais, I. G. N. Silva, B. J. Ferreira, A. C. Teixeira, S. P. Sree, H. Terraschke, F. A. Garcia, E. Breynaert, D. Mustafa, *Chem. Commun.* **2023**, *59*, 13571.
[8] C. Jing, B. Dong, A. Raza, T. Zhang, Y. Zhang, *Nano Mater. Sci.* **2021**, *3*, 47.
[9] L. Zhang, M. Shi, W. Zhou, W. Guan, C. Lu, *Anal. Chem.* **2021**, *93*, 7724.
[10] X. Wu, S. Feng, C. Mao, C. Liu, Y. Zhang, Y. Zhou, X. Sheng, *New J. Chem.* **2023**, *47*, 7093.
[11] Y. Ye, Y. Shan, H. Zhu, K. Chen, X. Yu, *RSC Adv.* **2023**, *13*, 2467.
[12] Q. Liu, Y. Zhang, Y. Zhou, M. Wang, R. Li, W. Yue, *J. Solid State Electrochem.* **2023**, *27*, 797.
[13] J. Mi, S. Liu, Z. Duan, Y. Fu, C. Lü, *Mater. Lett.* **2023**, *336*, 133845.
[14] A. S. Roy, S. K. Pillai, S. S. Ray, *ACS Omega* **2023**, *8*, 8427.
[15] N. Baiga, M. Sajidb, T. Environ, *Anal. Chem.* **2017**, *16*, 1.
[16] Z. Tan, *Energy Fuels* **2020**, *34*, 8939.
[17] K. Tadanaga, Y. Furukawa, A. Hayashi, M. Tatsumisago, *J. Electrochem. Soc.* **2012**, *159*, B368.
[18] Y. Cao, D. Zheng, F. Zhang, J. Pan, C. Lin, *J. Mater. Sci. Technol.* **2022**, *102*, 232.
[19] M. Kahl, T. D. Golden, *Materials* **2021**, *14*, 7389.
[20] R. Gao, D. Yan, X. Duan, *Cell Rep. Phys. Sci.* **2021**, *2*, 100536.
[21] I. F. Costa, L. Blois, T. B. Paolini, I. P. Assunção, E. E. S. Teotonio, M. C. F. C. Felinto, R. T. Moura, Jr., R. L. Longo, W. M. Faustino, L. D. Carlos, O. L. Malta, A. N. Carneiro Neto, H. F. Brito, *Coord. Chem. Rev.* **2024**, *502*, 215590.
[22] A. N. Carneiro Neto, E. E. S. Teotonio, G. F. de Sá, H. F. Brito, J. Legendziewicz, L. D. Carlos, M. C. F. C. Felinto, P. Gawryszewska, R. T. Moura, Jr., R. L. Longo, W. M. Faustino, O. L. Malta, in *Handbook on the Physics and Chemistry of Rare Earths*, (Eds: J.-C. G. Bünzli, V.K. Pecharsky), Vol. *56*, Elsevier, Amsterdam, The Netherlands, **2019**, Ch. 310.
[23] A. Morais, F. O. Machado, A. C. Teixeira, I. G. N. Silva, E. Breynaert, D. Mustafa, *J. Alloys Compd.* **2019**, *771*, 578.
[24] I. G. N. Silva, A. F. Morais, B. C. Lima, F. A. Garcia, D. Mustafa, *Appl. Clay Sci.* **2020**, *199*, 105861.
[25] A. F. Morais, I. G. N. Silva, B. C. Lima, F. A. Garcia, D. Mustafa, *ACS Omega* **2020**, *5*, 23778.
[26] S. Gago, M. Pillinger, R. A. Sá Ferreira, L. D. Carlos, T. M. Santos, I. S. Gonçalves, *Chem. Mater.* **2005**, *17*, 5803.
[27] A. C. Teixeira, I. G. N. Silva, A. F. Morais, D. Mustafa, *J. Rare Earths* **2022**, *40*, 260.
[28] A. F. Morais, D. Nanclares, I. G. N. Silva, A. Duarte, F. A. Garcia, E. Breynaert, D. Mustafa, *Nanoscale* **2021**, *13*, 11781.
[29] D. Nanclares, A. F. Morais, T. Calaça, I. G. N. Silva, D. Mustafa, *RSC Adv.* **2021**, *11*, 24747.
[30] C. K. Xia, W. Sun, Y. Y. Min, K. Yang, Y. L. Wu, *Polyhedron* **2018**, *141*, 377.
[31] R. Cao, D. Sun, Y. Liang, M. Hong, K. Tatsumi, Q. Shi, *Inorg. Chem.* **2002**, *41*, 2087.
[32] X. Li, Y. Wang, Z. Ma, R. Zhang, J. Zhao, *J. Coord. Chem.* **2010**, *63*, 1029.
[33] M. R. Shimpi, L. Giri, V. R. Pedireddi, *Chem. Select* **2018**, *3*, 855.
[34] W. Clegg, J. M. Holcroft, *Cryst. Growth Des.* **2014**, *14*, 6282.
[35] J. J. Yang, X. Y. Yu, Y. H. Luo, H. Zhang, W. P. Gao, *Inorg. Chem. Commun.* **2015**, *61*, 16.
[36] L. Yang, Q. Wang, H. Yao, Q. Yang, X. Lu, Z. Wu, R. Liu, K. Shi, S. Ma, *Dalton. Trans.* **2022**, *31*, 8327.
[37] N. Ghanbari, H. Ghafuri, *Heliyon* **2023**, *17*, e20978.
[38] R. Soltani, R. Pelalak, M. Pishnamazi, A. Marjani, A. B. Albadarin, S. M. Sarkar, S. Shirazian, *Sci. Rep.* **2021**, *11*, 1609.
[39] Y. S. Jun, W. X. Xue, C. Z. Shan, W. J. Wang, S. Hua, T. Hayat, W. X. Ke, *J. Hazard. Mater.* **2017**, *321*, 111.
[40] W. Xia, G. Z. Guo, X. Q. Wu, Y. M. Yin, Y. P. Wu, S. Li, R. Chi, D. S. Li, *J. Solid State Chem.* **2024**, *336*, 124783.
[41] I. L. Karle, Y. B. R. D. Rajesh, S. Ranganathan, *J. Chem. Crystallogr.* **2005**, *35*, 835.
[42] I. L. Karle, Y. B. R. D. Rajesh, S. Ranganathan, *J. Chem. Crystallogr.* **2009**, *39*, 201.
[43] N. P. Martin, J. März, C. Volkringer, N. Henry, C. Hennig, A. Ikeda-Ohno, T. Loiseau, *Inorg. Chem.* **2017**, *56*, 2902.
[44] N. B. Beck, Z. Bai, J. P. Brannon, D. G. Martinez, D. Grödler, B. N. Long, T. N. Poe, B. M. Rotermund, T. E. Albrecht-Schönzart, J. M. Sperling, *Inorg. Chem.* **2022**, *61*, 17730.
[45] G. B. Rocha, R. O. Freire, N. B. Da Costa Jr, G. F. de Sá, A. M. Simas, *Inorg. Chem.* **2004**, *43*, 2346.
[46] G. Doungmo, A. F. Morais, D. Mustafa, T. Kamgaing, E. Njanja, M. Etter, I. K. Tonlé, H. Terraschke, *RSC Adv.* **2022**,*12*, 33469.
[47] X. Duan, D. Evans, J. He, Y. Kang, A. I. Khan, F. Leroux, B. Li, F. Li, D. O'Hare, R. C. T. Slade, C. Taviot-Gueho, M. Wei, G. Williams, *Struct. Bonding* **2006**, *119*, 3.
[48] J. H. S. Romero, G. P. Saito, F. Cagnin, M. A. Cebim, M. R. Davolos, *Opt. Mater.* **2022**, *124*, 111703.
[49] A. Ostasz, R. Lyszczek, L. Mazur, J. Sienkiewicz-Gromiuk, I. Rusinek, Z. Rzaczynska, *J. Anal. Appl. Pyrolysis* **2013**, *99*, 203.
[50] S. Marappa, P. Vishnu Kamath, *Z. Anorg. Allg. Chem.* **2015**, *641*, 927.
[51] G. F. de Sá, O. L. Malta, C. M. Donegá, A. M. Simas, R. L. Longo, P. A. Santa-Cruz, E. F. da Silva, Jr., *Coord. Chem. Rev.* **2000**, *196*, 165.
[52] A. N. Carneiro Neto, R. T. Moura Jr., A. Shyichuk, V. Paterlini, F. Piccinelli, M. Bettinelli, O. L. Malta, *J. Phys. Chem. C* **2020**, *124*, 10105.
[53] V. Paterlini, F. Piccinelli, M. Bettinelli, *Physica B* **2019**, *575*, 411685.
[54] L. P. Wu, M. Munakata, T. Kuroda-Sowa, M. Maekawa, Y. Suenaga, *Inorg. Chim. Acta* **1996**, *249*, 183.
[55] C. Y. Sun, X. L. Wang, X. Zhang, C. Qin, P. Li, Z.-M. Su, D. X. Zhu, G. G. Shan, K. Z. Shao, H. Wu, J. Li, *Nat. Commun.* **2013**, *4*, 2717.
[56] X. Yu, A. A. Ryadun, D. I. Pavlov, T. Y. Guselnikova, A. S. Potapov, V. P. Fedin, *Adv. Mater.* **2024**, *36*, 2311939.
[57] L. L. da Luz, B. F. Lucena Viana, G. C. Oliveira da Silva, C. C. Gatto, A. M. Fontes, M. Malta, I. T. Weber, M. O. Rodrigues, S. Alves Jr, *Cryst. Eng. Commun.* **2014**, *16*, 6914.
[58] M. Latva, H. Takalo, V. M. Mukkala, C. Matachescu, J. C. Rodriguez-Ubis, J. Kankare, *J. Lumin.* **1997**, *75*, 149.